Available online at www.sciencedirect.com

SciVerse ScienceDirect

Energy Procedia 24 (2012) 351 – 362

Energy Procedia

DeepWind, 19-20 January 2012, Trondheim, Norway

Effects of hydrodynamic modelling in fully coupled simulations of a semi-submersible wind turbine

Marit I. Kvittem[a,b], Erin E. Bachynski[b], Torgeir Moan[b]

[a]*NOWITECH, NTNU, NO-7491 Trondheim, Norway*
[b]*Centre for Ships and Ocean Structures, NTNU, NO-7491 Trondheim, Norway*

Abstract

This work examines the dynamic response of a single semi-submersible wind turbine (SSWT) based on different hydrodynamic theories. Comparisons of platform motions and structural responses in the wind turbine are shown for simulations for a model with linear potential flow solution and quadratic drag and simulations with only Morison-type forces. The SSWT modelled in this study is based on WindFloat and carries the NREL 5MW wind turbine and should be considered a large volume structure. This implies that diffraction effects should be considered by using potential flow theory and viscous effects by Morison's equation.

A new coupled simulation code was developed by linking the SIMO and RIFLEX hydrodynamic, structural, and control system computational tools, from MARINTEK, with the aerodynamic forces and wind field generation capabilities of AeroDyn and TurbSim, from NREL. In contrast to other available simulation codes, this combination enabled the implementation of these two different hydrodynamic theories and offered the possibility of finite element mooring line models. Wave-only simulations were considered first, in order to tune and compare potential theory versus the inertia term in Morison's equation. Some limited coupled wave-wind simulations give an indication of the extent to which hydrodynamic modelling affects the global response.

The SSWT case study showed that the Morison model with forces integrated up to wave elevation gave a good representation of the motions compared to the potential flow model with quadratic drag forces. It also showed that motions are sensitive to choice of added mass coefficients, stretching and dynamic pressure under the columns. Combined wind and wave simulations, using a non-optimized control approach, showed that pitch motions influence the power production and blade bending moments.

Keywords:
offshore wind energy, semi-submersible, integrated analysis, hydrodynamics

1. Introduction

The majority of commercial and academic software for analyzing floating wind turbines (FWTs) have been developed from analysis tools for onshore wind turbines. This often means that the software includes advanced aerodynamics and limited hydrodynamics. In many cases, the only hydrodynamics model is slender element theory with Morison-type forces on the submerged part of the structure. A few analysis programs for FWTs come from the offshore industry, often with advanced hydrodynamics but simplified aerodynamics. Certain concepts, such as the spar buoy FWT, are slender enough to justify the use of

 doi:10.1016/j.egypro.2012.06.118

Morison's equation [1] together with a simplified treatment of pressure that causes heave motion. For large volume structures such as barges or semi-submersibles, however, diffraction effects may be significant. On the other hand, applying Morison's equation makes it possible to account for non-linear effects that come from calculating the wave forces in the instantaneous position of the platform. These effects may also be important. The consequences of applying different hydrodynamic theories have not yet been studied due to limitations in analysis tools.

The Morison equation has been used as the hydrodynamic model for for semi-submersible wind turbine (SSWT) analysis before, by for instance Phuc and Ishihara [2]. They conclude that the Morison model compares well with model tests for a SSWT with slender elements in regular waves. This result cannot be assumed to hold for WindFloat and most other semi-submersibles with large-diameter elements, and must also be examined critically for irregular wave conditions. A code-to-code comparison for calculating motions of a 1/64 scale drill rig semi-submersible was conducted by the ITTC Ocean Engineering Committee [3]. Their conclusion was that both potential forces and viscous forces should be included in the analysis, and that the effect of wave height was large in heave.

In this work the effect of hydrodynamic load modelling for a single SSWT is investigated. The SSWT design under consideration is very similar to the WindFloat concept [4]. Since a proper description of hydrodynamic loads requires both potential theory and viscous drag, quadratic drag elements are included in both models presented here. For simplicity, the drag coefficients are the same for both the potential and the Morison model. Added mass coefficients were calculated based on the frequency dependent added mass from the potential theory solution. After coefficients were found, regular and irregular wave analyses were performed for both the Morison model and the potential theory model, and response characteristics were investigated and compared. Limited analyses with an operating turbine and turbulent wind load were run to study the effect of hydrodynamic modelling on power production.

2. Methodology

2.1. Potential Theory and Morison's Equation

Two practical options for hydrodynamic load calculation in a global analysis are potential flow theory and Morison's equation. The first order potential flow theory applied here considers the solution of a linearized boundary value problem for inviscid, incompressible flow about a rigid body. This approach, using a panel method solution, accounts for Froude-Krylov forces and diffraction effects for large volume structures. The resulting solution is frequency-dependent and linear with respect to wave amplitude.

Morison's equation is a semi-empirical method for calculating wave loads on slender structures. For a fixed cylindrical pile, Morison's equation is equivalent to the potential flow solution when the wavelength to diameter (λ/D) ratio is large and viscous effects are negligible [5]. Morison's equation does not, however, account for diffraction effects, which, as a rule of thumb for fixed cylinders, are important for wavelengths shorter than five times the diameter [6]. Furthermore, the Morison formulation is extended to non-slender members, including, for example, the heave plates of the semi-submersible in this study. Due to the quadratic drag force and the formulation in terms of relative velocities and accelerations, Morison's equation is solved in the time domain with frequency-independent coefficients.

Although we are interested in a coupled multiple degree-of-freedom (DOF) system, let us consider the time-domain equation of motion for a floating single DOF system in order to compare these hydrodynamic models. According to pure potential flow theory, the single DOF system takes the form of Eq. 1 [7]:

$$(M + A_\infty)\ddot{x}(t) + \int_{-\infty}^{\infty} \kappa(t-\tau)\dot{x}(\tau)d\tau + Cx(t) + K\left(x(t)\right) = F^{FK} + F^{D} \tag{1}$$

where M is the dry mass, A_∞ is the added mass for high frequencies, $x(t)$ is the system displacement, $\kappa(t-\tau)$ is retardation function accounting for frequency-dependent added mass and damping, C is the hydrostatic restoring force, F^{FK} is the Froude-Krylov force and F^{D} is diffraction force. The first and second time derivatives are expressed by $\dot{x}$ and $\ddot{x}$. In practice, we also include a quadratic damping term (C_q) to approximate viscous effects, as well as non-linear restoring forces ($K(x(t))$) from the mooring system. The

quadratic damping term depends on the difference between the water particle velocity (u) and the body velocity. The resulting equation of motion for potential flow including viscous drag is then:

$$(M + A_\infty)\,\ddot{x}(t) + \int_{-\infty}^{\infty} \kappa(t-\tau)\dot{x}(\tau)d\tau + Cx(t) + K\,(x(t)) = F^{FK} + F^{D} + C_q|u - \dot{x}|\,(u - \dot{x}) \tag{2}$$

The same system, including nonlinear restoring forces, according to Morison-type wave loading is expressed by Eq. 3, where we have the same quadratic damping and no retardation function [7].

$$M\ddot{x}(t) + Cx(t) + K\,(x(t)) = (\rho_w V + m_a)a - m_a\ddot{x} + C_q|u - \dot{x}|\,(u - \dot{x}) \tag{3}$$

In Eq. 3, we have introduced the density of water (ρ_w), the volume of displaced water (V), a constant added mass (m_a), and the water particle acceleration (a).

Examining these two formulations, we can see that it is possible to tune the Morison equation coefficients to obtain identical responses for a single DOF system in regular waves of constant amplitude. The Morison model cannot, however, necessarily capture the equivalent hydrodynamic coupling effects for a multiple DOF system as in the potential flow formulation. Furthermore, the frequency-dependence and linear damping contributions are lost. On the other hand, the potential flow formulation does not consider wave particle accelerations above the waterline, and requires solving the Cummins equation, which introduces some computational cost. The applicability of these theories to the considered platform, which is described in the following section, is considered in greater detail in Section 2.3.

2.2. Single Semi-submersible Wind Turbine

The model investigated in this study is a semi-submersible substructure very similar to WindFloat [4], with the NREL 5MW turbine [8] (see Fig. 2.2) and OC3 tower [9]. The SSWT is modeled in SIMO/RIFLEX, a tool for coupled analysis of moored floating structures. Mooring lines, tower and blades are modeled by flexible RIFLEX elements, while the floating body is modeled as rigid in SIMO, with linear hydrostatic stiffness and coupled frequency-dependent added mass and linear damping. The force and motion transfer functions and retardation functions are calculated with Wadam [10] potential theory software. SIMO has the option to attach elements with Morison force model to the body, which was done here to add quadratic drag. In the Morison model, the added mass, damping and force transfer functions are set to zero, while both acceleration terms (added mass) and quadratic damping terms from Morison's equation are included.

In both models, the non-dimensional vertical drag coefficient, $C_D = 2C_q/\rho A^{proj}$, for the heave plate is given in [4] as 7.5 and we assume a horizontal drag coefficient of 1.0 for the columns based on DNV-RP-C205 [11]. As a first comparison of the models, Table 1 lists the natural periods of the system found by decay analyses for potential theory and for Morison equation with $C_a = 1.0$ for both columns and heave plates.

Fig. 1: WindFloat (courtesy of Principle Power)

Mode	Panel T (s)	Morison T (s)
Surge	99.8	97.3
Heave	19.9	21.4
Pitch	39.9	40.7

Table 1: Damped natural periods, assuming $C_a = 1.0$ for both horizontal and vertical Morison forces. $C_D = 7.5$ for heave plates and $C_D = 1.0$ for columns.

Four different variations of the Morison model were studied: pure Morison forces as in Eq. 3, with forces integrated up to mean water level (1) or up to wave elevation (2), pure Morison including the effect of calculating forces at instantaneous position (3), and Morison with a correction for dynamic pressure under the columns (4). Due to the surface piercing elements, this dynamic pressure correction gives a better representation of the forces in the vertical plane. This correction in Morison model (4) is implemented via an analytically derived force transfer function applied to the platform in SIMO.

2.3. Added Mass Coefficients

The dimensional added mass (m_a) for the Morison model is computed as in Eq. 4 for horizontal forces on the columns and Eq. 5 for vertical forces on the heave plates. In Eqs. 4- 5, R is the radius of the column or plate and L is the length of the column. Similar equations are found in [12] and [13] for cylinders and caissons, respectively. The values of the coefficients C_a must be tuned for different wave frequencies.

$$m_a^{hor} = \rho_w C_a^{hor} \pi R_{col}^2 L_{col} \tag{4}$$

$$m_a^{ver} = \rho_w C_a^{ver} \frac{2\pi}{3} R_{plate}^3 \tag{5}$$

Table 2 shows the range of wave cases considered. The wave heading is normal to the rotor plane (that is, in the x direction) as displayed in Fig. 2.2, hence only surge, heave and pitch motions are studied. These cases are applied in both regular and irregular waves, where for irregular waves the periods are peak periods and heights are significant heights. Morison added mass coefficients are calculated based on frequency dependent added mass from potential theory. Two of the cases are also run with wind loads for an operating turbine (see Tab. 3).

Table 2: Load cases

Wave period (s)	3.7	4.0	5.0	5.5	6.0	6.9	10.0	15.0	20.0	21.0
Wave height (m)	1.0	1.0	1.0	1.0	1.5	2.0	3.0	6.0	9.0	9.0

These load cases represent a range of different conditions, where different hydrodynamic effects may be of importance. The wave heights are selected to be appropriate for the given period. Figure 2 shows where the load cases in Tab. 2 are located in a theory validity diagram based on the cylinder diameter. The diagram is valid for a cylinder fixed to the ground [14], so it only gives an indication of which effects may be important for the freely floating body with multiple components. The conclusions drawn from Fig. 2 are that for wave periods 3.7 s to 6.0 s, diffraction may be important, while for periods 20 s and 21 s viscous drag may be important. Both Morison and diffraction theory may be applied to the intermediate cases, where inertial effects dominate.

2.4. Fully Coupled Analyses

In order to understand the impact of the different hydrodynamic theories on wind turbine simulation results, it is also important to consider the full floating system. Table 3 summarizes the two chosen wind-wave conditions: Condition 1, representing below-rated wind and gentle seas, and Condition 2, representing a typical operational condition. The wind fields, generated in TurbSim, correspond to the normal turbulence model (NTM) for class B of the IEC 61400-3 standard, with the power law applied for the shear profile [15]. At lower wind speed, the characteristic turbulence intensity is somewhat higher. The wave conditions were chosen to approximately correspond with the wind field characteristics according to typical North Sea conditions given by Faltinsen, 1990 [5].

Simulations for identical wind and wave time series were carried out for a land-based wind turbine (disregarding all wave input) and for two different hydrodynamic models: the potential flow theory with

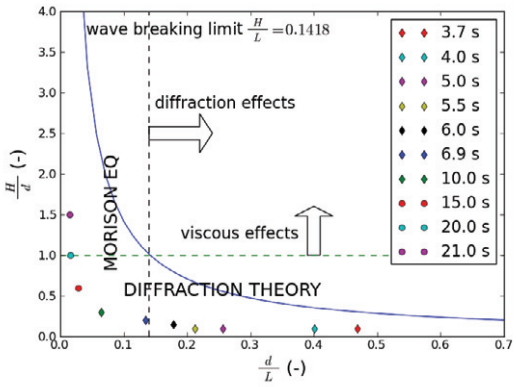

Fig. 2: Regions of validity of potential flow theory and Morison's equation (assuming fixed bodies) [14]

Table 3: Combined wind-wave simulation conditions

	Condition 1	Condition 2
Mean Wind Speed (90 m)	8 m/s	16 m/s
Power Law Exponent [15]	0.14	0.14
Characteristic Turbulence Intensity (90 m)	19.16 %	16.30 %
Significant Wave Height	1.5 m	6.0 m
Peak Wave Period	6.0 s	15.0 s
Simulation Length (excluding transient)	1800 s	1800 s

additional quadratic drag, and the pure Morison formula with integration up to the free surface (Morison model (2)), with coefficients as in Tab. 4. Wind and waves were applied in the x direction, i.e. normal to the rotor plane as displayed in Fig. 2.2.

The same generator torque and blade pitch control system were applied to all of the models, with the gains described in [8]. Floating systems generally require modifications to the control system in order to avoid negative feedback in over-rated wind conditions [16, 17], when the thrust force at the nacelle decreases for increasing relative wind speed. The horizontal velocity due to pitch at WindFloat's nacelle in these conditions is sufficiently low such that the destabilizing effect is small compared to the hydrodynamic damping, but an improved control system will be included in future work. It is also important to note that the aerodynamic model employed in these simulations does not account for dynamic wake effects, which may have important consequences for floating wind turbines due to the sheared inflow, which is exacerbated by the mean platform pitch. The dynamic wake option is available in the AeroDyn code for sufficiently high wind speed, but the BEM option with dynamic stall was applied here for consistency at different wind speeds.

3. Coupled Wind-Wave Simulation Tool

A new coupled simulation code (S-R-A) was developed by linking the SIMO [18] and RIFLEX [19] hydrodynamic, structural, and control system computational tools, from MARINTEK, with the aerodynamic forces and wind field generation capabilities of AeroDyn and TurbSim, from NREL [20]. The simulation tool employs the finite element solver available in the combined SIMO/RIFLEX tool, passing position and velocity information to the aerodynamic code via DLL at the first iteration of each time step. The DLL

returns lumped forces along the wind turbine blades. An external control system applies the generator torque according to a look-up table and blade pitch commands via PI control as in the NREL 5MW definition [8].

3.1. Finite Element Model

In the finite element model, the wind turbine tower is modeled with axisymmetric beam elements, while the blades consist of doubly symmetric cross sections. In contrast to the FAST model, the model includes the torsional degree of freedom of the blades. The control system, which is also coupled to the finite element program, applies appropriate torque directly to the low speed shaft and sets the angle of the rigid connection between the hub and blade root. Additional details regarding the wind turbine module of SIMO/RIFLEX (without AeroDyn and TurbSim) can be found in [21, 22].

3.2. Aerodynamic Model

The AeroDyn program provides both blade element momentum (BEM) and generalized dynamic wake (GDW) models for the aerodynamic force calculation [23]. The results shown in this paper employ the BEM method with the Beddoes dynamic stall model, but no dynamic wake effects.

3.3. Verification of Land-Based Wind Turbine Performance

Prior to using the S-R-A code for simulation of a floating offshore wind turbine, the global performance of a land-based wind turbine was compared against available tools such as FAST and HAWC2 [24]. Simulations of the NREL 5 MW wind turbine show good agreement regarding power production, rotor rotation, blade loads and deflections and tower loads. Fig. 3, as an example, compares several performance indicators for the FAST and S-R-A codes. The S-R-A results are shown for a fully flexible model and for a model with exaggerated torsional stiffness for the blades. As shown, the control pitch required at higher wind speeds decreases when the blades are flexible in torsion, in agreement with published results [25].

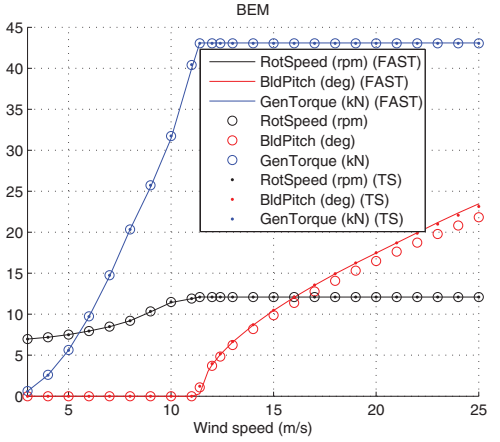

Fig. 3: Global performance indicators for the land-based NREL 5MW wind turbine. Rotor speed, blade pitch, and generator torque are compared for FAST, fully flexible RIFLEX-AeroDyn, and RIFLEX-AeroDyn with exaggerated torsional blade stiffness (indicated TS).

4. Results

4.1. Regular Wave Condition

First, added mass coefficients were calculated based on added mass from the potential theory solution, see Tab. 4. These coefficients were used for the Morison inertia forces in further analyses, if not stated otherwise. Figure 4 shows response amplitude operators (RAOs) using potential theory and four approaches

to Morison equation. Results shown in Fig. 4 are based on time domain analysis with regular waves, normalized with the input wave amplitude. The response outside the wave frequency was filtered out, so only linear wave excitation is included. The linear potential theory solution without quadratic drag is also shown. The wave heights used for these analyses are listed in Table 2. When quadratic drag is included, there is a quadratic relation between wave height and response, and this effect was not considered in this paper since the quadratic drag coefficients were the same for the two models.

Table 4: Coefficients calculated from Eq. 5 based on $A(\omega)$ from potential theory solution.

T_P (s)	3.7	4.0	5.0	5.5	6.0	6.9	10.0	15.0	20.0	21.0
C_a^{hor} (-)	0.51	0.76	0.65	1.05	1.35	1.18	1.07	1.06	1.03	1.03
C_a^{ver} (-)	0.88	0.88	0.88	0.88	0.89	0.89	0.90	0.91	0.91	0.91

From Fig. 4 it is clear that pure Morison with forces calculated up to mean water level overestimated heave and pitch motion compared to the potential theory and drag model, but by including forces up to wave elevation we got a good agreement. Correcting for dynamic pressure under the columns also gave a better fit, but this method can be improved by including forces up to wave elevation. For wave periods 20 and 21 seconds, surge motions for the modified Morison case were lower than the rest. This may be due to surge-pitch coupling effects. Calculating the forces at the instantaneous position did not have a significant effect for these cases.

Diffraction effects seemed to be important in heave response for periods lower than 6.9 s, which is in agreement with the theory validity diagram in 2.

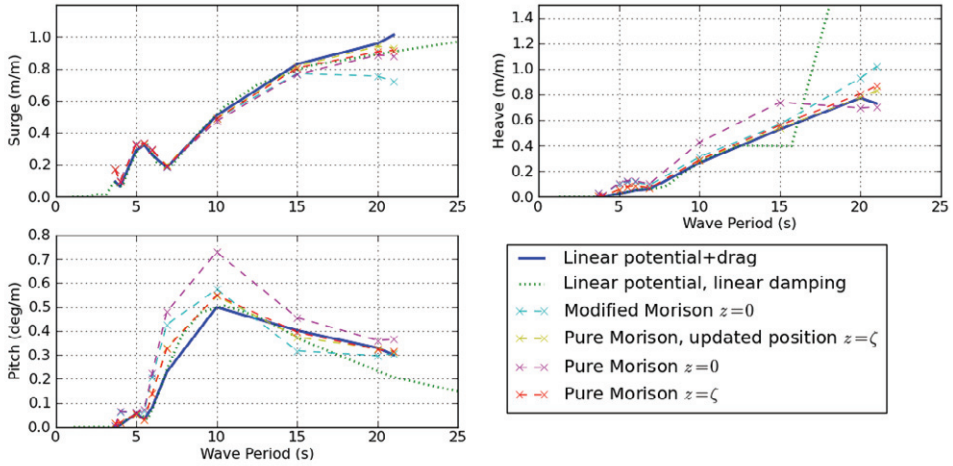

Fig. 4: Platform RAOs for surge, heave and pitch motion for variants of Morison and for potential and drag force. Inertial coefficients as in Table 4.

In addition, regular wave analyses with different horizontal (subscript h) and vertical (subscript v) inertial coefficients and integration of forces up to wave elevation were performed. The results are shown in Fig. 5, and it is clear that for each wave period the response in the potential theory model can be matched by choosing the correct coefficient. And the correct coefficients are not necessarily derived from the potential theory solution.

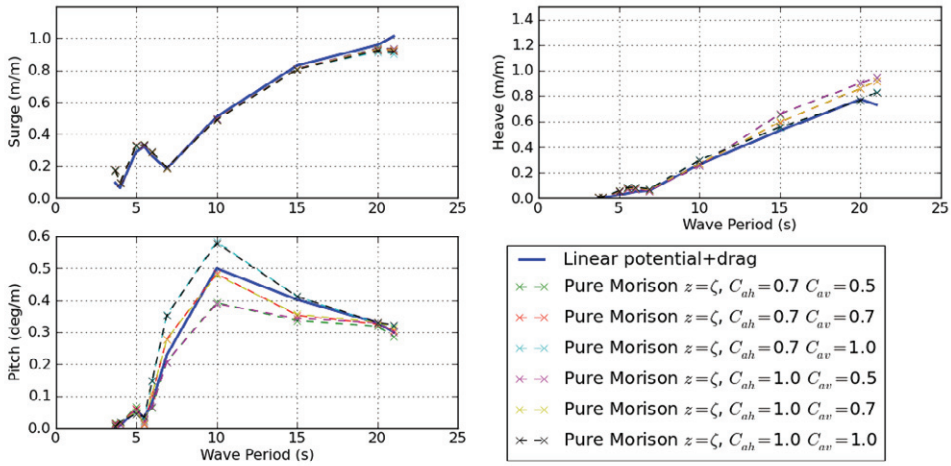

Fig. 5: Platform RAOs for surge, heave and pitch motion for pure Morison and for potential and drag force for different inertia coefficients

4.2. Irregular Wave Condition

After determining the coefficients in Tab. 4, the potential theory model and the pure Morison model with forces up to wave elevation were exposed to irregular wave conditions. Figure 6 shows the statistical properties of the irregular wave response for both the Morison model and the potential and drag model. Linear potential damping was equal to zero since it was significantly smaller than the drag damping. The wave time series was the same for both models in each load case. These results were based on one single time series per load case, where the simulation time is 30 minutes. This is not a sufficient statistical basis, but gives an indication of trends because the purpose is to compare between the Morison model and the potential plus drag model, and the wave time series are identical.

There was little difference in standard deviations in all degrees of freedom. The mean value of surge motion was higher for the Morison model than for the potential model for long wave periods. This may be due to the extra drift force caused by the inertia forces above mean water level acting on an asymmetric structure.

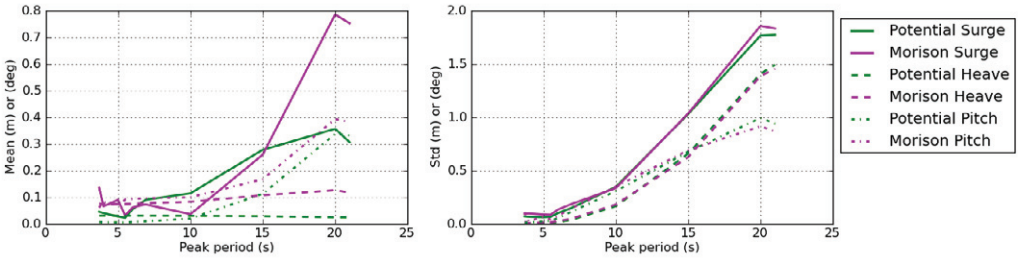

Fig. 6: Statistical properties for response to irregular waves with no wind

4.3. Turbulent Wind and Irregular Waves

A brief investigation of responses in turbulent wind and irregular wave conditions is presented here. One should note that these results correspond to limited stochastic analyses and that future work to reduce statistical uncertainties is planned.

Statistical results for the Condition 1 and 2 simulations are shown in Tables 5 and 6, respectively. In Condition 1, the wind forces were dominant, and the wind turbulence dominated the variability of all of the performance parameters. As shown in Table 5, there was very little statistical difference in the power production, turbine performance, blade loads, and floater motions when comparing simulations with the potential and Morison theory hydrodynamics models. The power production of the floating platform was, however, somewhat lower than that of the land-based tower. The reduction in power production of the floating platform compared to the land-based tower was in part due to the mean platform pitch, which decreases the efficiency of the energy harvesting, and also due to the pitch motion of the turbine, which followed the wind and reduced the relative velocity seen by the blades. The reduced mean power led to a corresponding decrease in power variability. The effect of the motions on the blade loads was also evident: there was a clear increase in the out-of-plane bending moment due to gravity effects. In-plane loads, which are dominated by gravity effects as the blades rotate, were not significantly affected by the floating platform motions.

Table 5: Wind-wave Condition 1 simulation statistics

	Land-Based		WF - Potential + Drag		WF - Morison	
	μ	σ	μ	σ	μ	σ
Electrical Power (kW)	1896	732	1774	619	1774	617
Generator Torque (kNm)	20.47	5.73	19.59	5.06	19.59	5.04
Blade Pitch (deg)	0	0	0	0	0	0
Rotor Speed (rpm)	9.39	0.96	9.24	0.83	9.23	0.83
Blade Root Out-Of-Plane Bending Moment (kNm)	5812	1450	5967	1550	5970	1571
Blade Root In-Plane Bending Moment (kNm)	596	2564	561	2513	561	2510
Surge (m)	n/a	n/a	11.59	2.85	11.94	3.09
Heave (m)	n/a	n/a	-0.01	0.03	0.04	0.03
Pitch (deg)	n/a	n/a	6.42	1.67	6.53	1.66

In Condition 2 (Table 6), the effects of the wave forces were more evident. As in Condition 1, the electrical power output from the floating turbines decreased compared to the land-based turbine. In contrast to Condition 1, however, the variability of the electrical power and generator torque increased for the floating platform. The power and generator torque varied slightly more for the Morison model than for the potential theory model, which can be attributed to the small increase in platform pitch motions.

Table 6: Wind-wave Condition 2 simulation statistics

	Land-Based		WF - Potential + Drag		WF - Morison	
	μ	σ	μ	σ	μ	σ
Electrical Power (kW)	4798	339	4767	384	4734	424.6
Generator Torque (kNm)	41.33	2.46	41.08	2.81	40.78	3.10
Blade Pitch (deg)	11.15	2.92	10.46	3.54	10.47	3.56
Rotor Speed (rpm)	12.10	0.25	12.09	0.27	12.09	0.30
Blade Root Out-Of-Plane Bending Moment (kNm)	5205	1645	5847	1850	5837	1900
Blade Root In-Plane Bending Moment (kNm)	1180	2621	1155	2524	1116	2510
Surge (m)	n/a	n/a	12.72	2.19	13.57	2.33
Heave (m)	n/a	n/a	-0.01	0.61	0.06	0.64
Pitch (deg)	n/a	n/a	7.18	1.87	7.37	1.96

To further demonstrate the differences between the hydrodynamic models when applied to coupled sim-

ulations, power spectra results from Condition 2 are shown in Fig. 7. The top left panel shows the wind in the global x direction measured at the hub for all three models as well as the wave elevation at the origin. The platform pitch for the two hydrodynamic models is shown in the second panel. As shown, the Morison model gave larger variation in platform pitch at both the wind and wave frequencies.

The low-speed shaft rotation speed (ω, shown in the third panel) is a complex result of the incoming wind, generator torque and blade pitch control actions, inertial effects, and platform motions. The controller is able to regulate the wind-driven variations (slower than 0.6 rad/s), but does not correct for variations in the wave frequency range. Thus, the differences in platform wave-induced motion can be seen in the rotation speed spectrum.

The blade 1 out-of-plane (OOP) bending moment is similarly difficult to dissect. The bending moment showed strong variation related to the blade pitch angle (not shown, but consistent between all three models) with large 1p variations. The platform pitch motion increased the amplitude of the 1p cycles, largely due to gravitational loading.

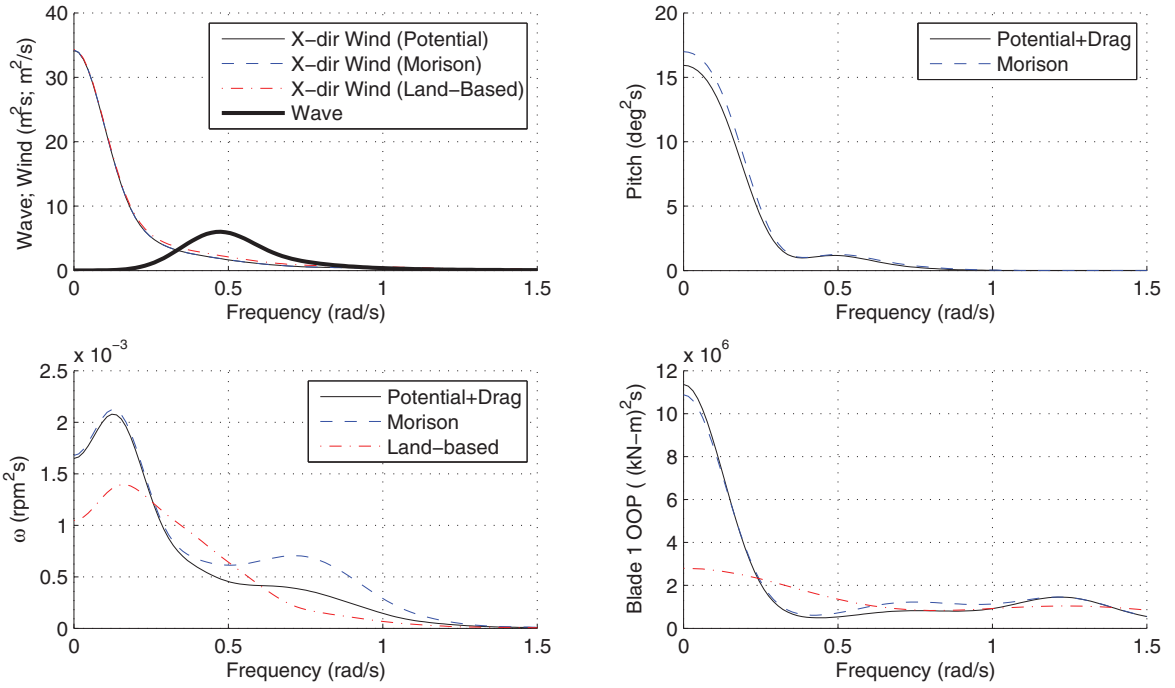

Fig. 7: Selected variance spectra: combined wind-wave Condition 2

5. Conclusions

A comparison of wave-induced response of a semi-submersible wind turbine using Morison equation and potential theory with Morison drag was performed by means of the analysis software SIMO/RIFLEX coupled to AeroDyn. First, added mass coefficients for the Morison equation were calculated based on the potential theory added mass. Then variations of models with wave forces from Morison's equation were run in regular and irregular wave analyses and compared to the potential theory solution. A sensitivity study on inertia coefficients was also performed. To study the effect of Morison versus potential theory on power production, fully coupled analyses with wind and waves were performed.

The results from these studies showed that it is possible to obtain the same response amplitudes in regular waves for periods above 7 seconds by choosing proper coefficients. For wave periods below 7 seconds, diffraction effects became important for heave motions. Surge motions were fairly insensitive to the choice of added mass coefficients. Results also showed that inertia coefficients directly calculated from the potential theory solution do not necessarily give the best agreement between Morison's equation and potential theory.

Pure Morison forces overestimated heave and pitch motion compared to the potential theory solution, but by including forces above mean water level good agreement was achieved. Also, adjusting pure Morison with dynamic pressure under the columns improved the results, though the method for including the dynamic pressure has potential for improvement. Calculating the forces at the updated position of the platform did not have a significant effect.

In the irregular wave analysis there were no significant differences between the two theories in the standard deviation of the motions. Differences in the mean surge motion were observed, which may be caused by inertial forces above the mean water level acting on an asymmetric structure.

Pitch motions decreased the relative wind velocity seen by the turbine blades and led to a decrease in power efficiency compared to a land-based turbine. As a consequence of larger pitch motions predicted with the Morison model than with the potential flow model, the predicted power production was more variable than in the potential theory model.

Having analysis software capable of describing advanced hydrodynamics is important when studying large volume structures, but for this particular semi-submersible the findings showed that slender body theory by Morison is sufficient for the wave periods between 7 and 21 seconds. The coupled simulation tool made it possible to study the impact of pitch motions on power production and blade bending moments, which showed to be significant. A better control strategy is required to improve the power performance and reduce the pitch motions of the platform. Large pitch motions influence extreme loads, fatigue life and power production of the system, so having a good prediction of responses to wind and waves is crucial.

References

[1] M. Karimirad, Z. Gao, T. Moan, Dynamic motion analysis of catenary moored spar wind turbine in extreme environmental condition, in: Proceedings of the European Offshore Wind Conference, Sweden, 2009.

[2] P. V. Phuc, T. Ishihara, A study on the dynamic response of a semi-submersible floating offshore wind system part 2: Numerical simulation, in: Proceedings of the International Conferences of Wind Engineering 12, Cairns, Australia, 2007.

[3] M. Takagi, A comparison of methods for calculating the motion of a semi-submersible, Ocean Engineering 12 (1) (1985) 45–97.

[4] D. Roddier, A. Peiffer, A. Aubault, J. Weinstein, A generic 5MW WindFloat for numerical tool validation and comparison against a generic spar, in: Proceedings OMAE 2011, 2011, paper no. OMAE2011-50278.

[5] O. M. Faltinsen, Sea Loads on Ships and Ocean Structures, Cambridge University Press, 1990.

[6] N. Barltrop, Floating Structures: A Guide for Design and Analysis, 1998.

[7] MARINTEK, SIMO Theory Manual (2009).

[8] J. Jonkman, S. Butterfield, W. Musial, G. Scott, Definition of a 5-MW reference wind turbine for offshore system development, Tech. rep., NREL, NREL/TP-500-38060 (2009).

[9] J. Jonkman, Definition of the Floating System for Phase IV of OC3, Tech. rep., National Renewable Energy Laboratory (2010).

[10] Det Norske Veritas, SESAM User Manual Wadam (2008).

[11] Det Norske Veritas, Environmental conditions and environmental loads, Tech. Rep. DNV-RP-C205 (2007).

[12] N. Clauss, E. Lehmann, C. Ostergaard, Offshore Structures - Conceptual design and Hydromechanics, 1988.

[13] S. Chakrabarti, Added mass and damping of a TLP column model, in: Proceedings of the Offshore Technology Conference, Houston, Texas, 1990, pp. 559–571.

[14] M. M. Bernitsas, Viscous forces on circular cylinders in separated flows. case study: Cable strumming., lecture Notes for NA 621 (1982).

[15] International Electrotechnical Commission, Wind turbines - Part 3: Design requirements for offshore wind turbines, Tech. Rep. IEC61400-3 (2009).

[16] T. J. Larsen, T. D. Hanson, A method to avoid negative damped low frequent tower vibrations for a floating, pitch controlled wind turbine, Journal of Physics: Conference Series, The Second Conference on The Science of Making Torque from Wind 75.

[17] J. M. Jonkman, Influence of control on the pitch damping of a floating wind turbine, in: Proceedings of the 2008 ASME Wind Energy Symposium, no. NREL/CP-500-42589, 2008.

[18] MARINTEK, SIMO User's Manual (2007).

[19] MARINTEK, RIFLEX User's Manual (2009).

[20] National Renewable Energy Laboratory - National Wind Technology Center, NWTC design codes (nov 2011). URL `http://wind.nrel.gov/designcodes/`

[21] H. Ormberg, E. Passano, N. Luxcey, Global analysis of a floating wind turbine using an aero-hydro-elastic model: Part 1: Code development and case study, in: Proceedings of the 30th International Conference on Ocean, Offshore, and Arctic Engineering, Rotterdam, the Netherlands, no. OMAE2011-50114, 2011.
[22] N. Luxcey, H. Ormberg, E. Passano, Global analysis of a floating wind turbine using and aero-hydro-elastic numerical model. Part 2: Benchmark study, in: Proceedings of the 30th International Conference on Ocean, Offshore, and Arctic Engineering, Rotterdam, the Netherlands, no. OMAE2011-50088, 2011.
[23] P. J. Moriarty, A. C. Hansen, AeroDyn theory manual, Tech. Rep. NREL/TP-500-36881 (2005).
[24] T. J. Larsen, How 2 HAWC2, the user's manual, Tech. Rep. Risø-R-1597(ver. 3-9) (2009).
[25] J. Jonkman, W. Musial, Offshore code comparison collaboration (OC3) for IEA Wind Task 23 offshore wind technology and deployment, Tech. Rep. NREL/TP-5000-48191, National Renewable Energy Laboratory (2010).